Applied Catalysis B: Environmental 150–151 (2014) 389–395

Contents lists available at ScienceDirect

Applied Catalysis B: Environmental

journal homepage: www.elsevier.com/locate/apcatb

# Effect of the type of acid used in the synthesis of titania–silica mixed oxides on their photocatalytic properties

B. Llano [a,*], M.C. Hidalgo [b], L.A. Rios [a], J.A. Navío [b]

[a] Departamento de Ingeniería Química, Facultad de Ingeniería, Universidad de Antioquia UdeA, Calle 70 No. 52-21, Medellín, Colombia
[b] Instituto de Ciencia de Materiales de Sevilla (ICMS), Centro Mixto CSIC-Universidad de Sevilla, C/Américo Vespucio 49, Sevilla 41092, Spain

ARTICLE INFO

*Article history:*
Received 11 September 2013
Received in revised form
10 November 2013
Accepted 20 December 2013
Available online 30 December 2013

*Keywords:*
$TiO_2$–$SiO_2$
Phenol oxidation
Photocatalysis
Acid treatment
Anatase–rutile–brookite

ABSTRACT

$TiO_2$–$SiO_2$ mixed oxides were synthesized by the sol–gel technique using three different acids, i.e., acetic, sulfuric, or chlorhydric acid. Their photocatalytic behavior was evaluated on the phenol oxidation in liquid phase and correlated with the characterization results. It was found that the kind of acid used during the preparation strongly influences the phase composition and stability of the $TiO_2$ phases incorporated in the silica structure as well as the photocatalytic activity. In all cases, silica introduced a dispersive effect that stabilized the $TiO_2$ crystalline phases upon calcination at 700 °C. $SO_4^{2-}$ and $CH_3COO^-$ ions stabilized the anatase phase at high calcination temperatures (700 °C) leading to samples with the highest photoactivities. $Cl^-$ ions induced the formation of traces of rutile and brookite resulting in a lower photoactivity. The highest photoactivity was achieved with the catalyst synthesized with acetic acid and calcined at 700 °C (TS1-700-ace). The photocatalytic performance of this material was even better than that obtained with the commercial catalyst Degussa P-25.



## 1. Introduction

Photocatalytic degradation of pollutants with $TiO_2$ has become one of the most promising technologies to protect the environment. One of the challenges currently faced by photocatalysis is the optimization of $TiO_2$ in such a way that photocatalysis will be more applicable at a practical level [1]. The three main polymorphs of $TiO_2$, i.e., anatase, brookite, and rutile, exhibit different physical properties such as refractive index, chemical and photochemical reactivity which in turn are closely related with the crystalline structure, morphology, and particle size.

In most of the research works on the topic, the crystalline anatase phase appears to be more photoactive than rutile and brookite. The difficulty to obtain pure anatase phase lies in the fact that rutile is the polymorph thermodynamically more stable, and although anatase is kinetically stable it is easily transformed into rutile at temperatures ranging from 500 to 1000 °C [2]. According to that, the development of new methods of synthesis in which the shape, size, and $TiO_2$ crystalline phases can be controlled is an important task to be achieved in the field of photocatalysis [3].

It has been reported that the kind of acid catalyst used in the synthesis of $TiO_2$ dramatically affects the crystallization process, inducing the formation of one or another phase. In this regard, acids like HCl or $HNO_3$ induce the formation of brookite and rutile and even a mixture of the three phases, whose relative proportions depend on the range of acidity, temperature, titanium concentration, and reaction time [4,5]. It is difficult to obtain pure brookite phase and it is usually synthesized in combination with other crystalline phases [6].

On the other hand, it has also been found that acid peptization with sulfuric acid retards the transition from anatase to rutile and, in addition, sulfated titanium oxide exhibits a highlighted photocatalytic activity [7–9]. The remarkable behavior displayed by sulfated materials has been ascribed to their large surface area, anatase crystalline phase, and the increment of the acid properties. Colón et al. [10] have established that sulfate ions stabilize the anatase phase up to 700 °C, obtaining highly defective materials due to the creation of oxygen vacancies through a dehydroxilation process of an excess of adsorbed protons. The loss of surface oxygen ions as well as the predominant anatase phase seems to be the determinant factors for the high photocatalytic activity showed by sulfated materials, improving the charge carrier's separation and the diffusion of the same to the surface [10].

Li et al. [11] studied the effect of the $SO_4^{2-}$ dopant over $TiO_2$ synthesized by the sol–gel method under supercritical and

* Corresponding author. Tel.: +574 2196587; fax: +574 2196565.
*E-mail addresses:* ebala482@udea.edu.co, bivianaastrid@gmail.com (B. Llano).

0926-3373/$ – see front matter © 2013 Elsevier B.V. All rights reserved.
http://dx.doi.org/10.1016/j.apcatb.2013.12.039

conventional conditions of drying, and also evaluated the photocatalytic properties of the oxides on the phenol degradation. The obtained results showed that the most influent factors over the photocatalytic properties of the $SO_4^{2-}/TiO_2$ oxides were the presence of pure anatase phase, high surface area, large pore volume and pore size, crystalline defects (oxygen vacancies), and specially the surface acidity.

Moreover, it is well known that the addition of ligands or modifying compounds such as β-diketones (e.g., acetylacetone) or carboxylic acids (acetic acid) allows to control the hydrolysis reaction rate of titanium alkoxides (highly reactive) in the sol–gel synthesis, avoiding the precipitation of undesirable phases. In this sense, acetic acid is usually employed as modifying or stabilizing agent in the sol–gel synthesis, since this compound reacts chemically with the titanium alkoxide at atomic level to give a new precursor. The steric effect of the acetate ligand and the increase in the number of coordination of Ti lead to a decrease in the rate of the hydrolysis reaction [12–14].

In the last years, titania–silica mixed oxides have become a new alternative in photocatalytic processes. Their main applications are based on the ability to act as catalyst and support in a wide variety of reactions. They exhibit characteristic properties from both single oxides such as photocatalytic activity, high surface area, thermal stability, and mechanical strength. In addition, as a result of the interaction between $SiO_2$ and $TiO_2$ at atomic level synergic effects are generated including quantum size and support effect as well as the formation of new catalytic acid sites [15–18].

$TiO_2$, especially in its anatase crystalline form, is the most widely used material in studies of photocatalytic degradation. However, aspects such as particle size and poor surface area have motivated the development of supported systems in which $SiO_2$ has emerged as an appropriate support for improving the photocatalytic process, since it is a chemically inert material with large surface area and transparent to UV radiation.

In this study $TiO_2$–$SiO_2$ were synthesized by the sol–gel technique and the effect of three different acids on the phase composition and photocatalytic activity was studied. In addition, the effect of calcining the samples at 500 and 700 °C was also investigated. The photocatalytic behavior was evaluated on the phenol oxidation in liquid phase and correlated with the obtained characterization results. The influence of silica on the crystalline phases and its role as a retarding agent in the crystallization process was also established.

## 2. Experimental

### 2.1. Catalyst preparation

$TiO_2$–$SiO_2$ mixed oxides were synthesized through the sol–gel technique using tetraethoxysilane (TEOS, Aldrich 98%) and titanium tetraisopropoxide (TTIP, Aldrich 97%) as silica and titania sources, respectively. The synthesis procedure involved two stages of hydrolysis of each alkoxide. In the first step, the hydrolysis of TEOS in isopropanol was performed by adding distilled water previously acidified with acetic, sulfuric, or chlorhydric acid, under the following molar ratios: TEOS:water:isopropanol:acid = 1:20:8:0.4. The solution was then left at room temperature for 14 h to promote hydrolysis and gelation of the silicon alkoxide. In the second step, the hydrolysis of a solution of TTIP in isopropanol was carried out by adding acidified distilled water. Final molar relation TTIP:water:isopropanol:acid was 1:12:14:1. After gelation time, the two solutions were mixed to obtain a transparent $TiO_2$–$SiO_2$ sol and it was stirred for 1 h at room temperature. After that, heating at 65 °C was carried out to obtain a transparent gel. Additional drying at 110 °C was performed to allow the formation of a xerogel structure. The xerogel was ground into fine powders and calcined at 500 and 700 °C for 2 h in static air. The molar ratio Ti/Si was 1. The samples were labeled as TS1-CT-acid, where TS1 is referred to titania silica (Ti/Si = 1), CT is the calcination temperature (500 or 700 °C) and the word acid is associated with the type of acid used in the synthesis, i.e., ace (acetic), sul (sulfuric), and clor (chlorhydric). $SiO_2$ blank was also synthesized under the same conditions, avoiding the addition of the titania source, in order to make some comparisons.

### 2.2. Characterization of the catalysts

XRD patterns were obtained on a Siemens D-501 diffractometer with Ni filter and graphite monochromator, using Cu Kα radiation (λ = 1.5418 Å). Crystallite sizes of the different phases were estimated from the line broadening of the corresponding X-ray diffraction peaks using the Scherrer equation. Peaks were fitted using a Voigt function.

BET surface area and porosity measurements were performed using a Micromeritics Gemini V, by means of $N_2$ adsorption at 77 K. Prior to the analysis, the samples were degassed under $N_2$ flowing at 100 °C for 2 h, followed by a vacuum treatment at the same temperature for 1 h.

Thermogravimetric analyses and differential thermal analyses (TGA/DTA) were recorded using a STA 1600 Platinum Series instrument (LINSEIS).

Infrared (IR) spectra of the materials were recorded with a Varian 660 spectrometer, using KBr pellets as matrix for the powder samples.

UV–vis diffuse reflectance absorption spectra were acquired with a Varian spectrometer model Cary 100 equipped with an integrating sphere, using $BaSO_4$ as reference. All the spectra were recorded in diffuse reflectance mode. Since the Kubelka Munk function can be considered proportional to the radiation absorption, the bandgaps were calculated from the spectra recorded by plotting $(F(R)h\nu)^{1/2}$ vs. $h\nu$, according to the method proposed by Tandom and Gupta [19].

The isoelectric points of the catalysts were not measured. But, it has been reported that the isoelectric points of these kind of materials are located around 4–6. Due to the fact that the silica creates Lewis acid sites, the isoelectric points of $SiO_2$-modified $TiO_2$ oxides are lower than those of pure $TiO_2$ and decrease with increasing $SiO_2$ content [20]. The surface charge of the photocatalyst can influence the adsorption of phenol (pKa 9.95 at 25 °C). Brezová et al. and Chiou et al. [21,22] found that for $TiO_2$ the degradation of phenol is very effective in mild acidic solutions and that between pH 2.0 and 10 only small changes in the phenol degradation rates were observed. Because of this, all the experiments were carried out under autogenous pH of the phenol solution (pH 5.5).

### 2.3. Photocatalytic experiments

The photocatalytic activity of the prepared samples was tested through the phenol oxidation in water (50 ppm) at a catalyst concentration of 1 g/L, in a Pyrex immersion well reactor. The UV light source was provided by a medium pressure Hg lamp (400 W) supplied by Applied Photophysics, which has a main emission line of 365 nm. The lamp was placed inside the batch reactor surrounded by a double borosilicate glass jacket where a water stream keeps the temperature of the solution constant. During the photooxidation process (2 h), an oxygen flow was used to maintain homogeneously suspended the catalyst in the solution. Samples of 2 mL volume were withdrawn at different time intervals, then filtered (Millipore Millex25 0.45 μm membrane filter) and analyzed by UV–vis spectrometry at 270 nm (characteristic phenol band). Prior to exposure to UV light, the photocatalysts were mixed with the phenol solution

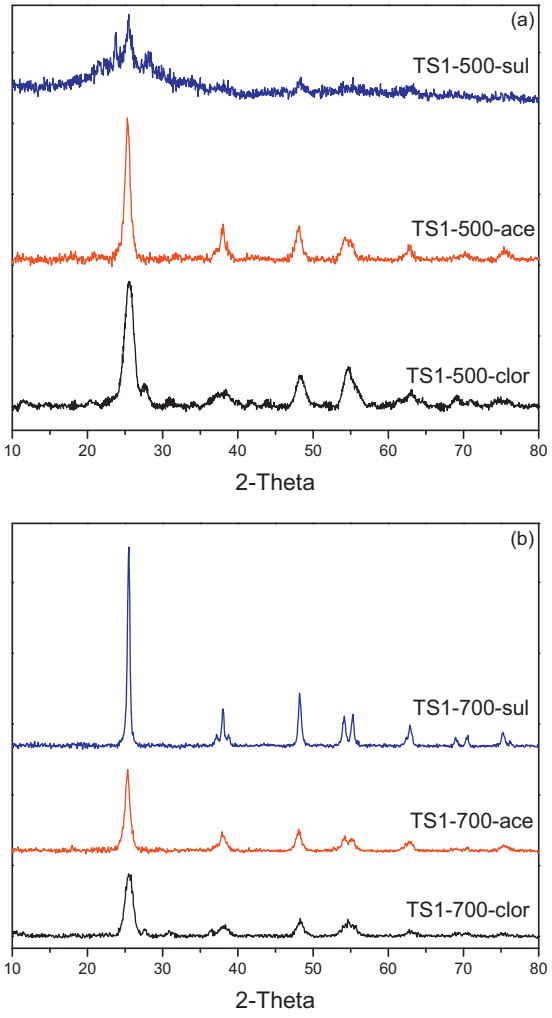


**Fig. 1.** X-ray diffraction patterns of the indicated samples calcined at: (a) 500 °C, (b) 700 °C.

for 15 min in the dark. It was assumed zero order kinetics in the first stages of the photooxidation process (20 min); so the degradation rates were obtained from the slopes of the conversion plots. In all cases, the regression coefficients were higher than 0.995.

## 3. Results and discussion

### 3.1. Characterization of the $TiO_2$–$SiO_2$ mixed oxides

XRD patterns of the samples calcined at 500 and 700 °C are shown in Fig. 1. It can be inferred that $TiO_2$ incorporated into the silica is in crystalline state, except in the sample TS1-500-sul, where together with an incipient anatase phase, a high amount of amorphous phase can also be found. Silica is in amorphous phase and there are no peaks belonging to silica or silicates in any of the oxides.

Mixed oxides synthesized with hydrochloric acid contain the anatase crystalline phase but with traces of brookite and rutile. The calcination temperature does not significantly affect the crystalline phases and the same ratio of phases is clearly observed at 500 and 700 °C. Stabilization of the anatase phase can be ascribed to the dispersive effect of silica which avoids mutual contact among $TiO_2$ particles, decreasing particle nucleation and the consequent growth of rutile crystallites, controlling in this way the process of phase transition.

Mixed oxides TS1-500-ace and TS1-700-ace exhibit the anatase as the only crystalline phase, this could be ascribed to the presence of the acetate ligand that stabilizes the anatase phase at temperatures above 500 °C and to the dispersive effect of silica. Catalyst TS1-500-sul is mainly amorphous because at that temperature (500 °C) the sulfate groups still remain in the oxide structure and it has been demonstrated that they inhibit the crystallization process [10]. However, at 700 °C the crystallization process is completed and a highly crystalline anatase phase is obtained. Results show that $Cl^-$ ions induce the formation of rutile and brookite, while $SO_4^{2-}$ and $CH_3COOH^-$ anions favor the formation of pure anatase. These results are in agreement with previous studies reported for pure $TiO_2$ oxides [23].

Table 1 shows a summary of some of the characterization results. The size of the anatase crystallites, calculated by the Scherrer equation, increases just slightly when the calcination temperature changes from 500 to 700 °C, which is consistent with a sinterization process. It can be observed that the crystallite size depends on the type of acid, but at the same time, it correlates with the degree of crystallinity of each sample. Thus, sample TS1-700-sul, the best crystallized catalyst, shows the highest crystallite size of all samples. These results clearly show the stabilizing role of silica on the crystallite growth of the mixed oxides.

BET surface areas are also shown in Table 1. Mixed oxides have high surface areas, especially those synthesized with hydrochloric acid. Materials obtained from acetic acid have areas of 349 and 320 $m^2/g$ for calcination temperatures of 500 and 700 °C, respectively. Samples obtained with sulfuric acid exhibit an atypical behavior since the surface area increases with increasing calcination temperature. This increase in surface area is accompanied by an increase in pore volume and diameter. One possible explanation for this behavior is that during the sol–gel synthesis with this acid sulfate groups are located in the pores of the catalyst structure. Since these groups are completely lost above 650–700 °C, calcining the sample until 700 °C causes an increase in surface area compared with the sample calcined at 500 °C. While at 500 °C some $SO_4^{2-}$ groups were occluding the mesopores, at 700 °C these groups have been removed, leaving the pores free and also protected from the effects of heat treatment. The pore volume markedly increases with the temperature of calcination, which is consistent with what has been above stated. Surface area of the $SiO_2$ blank is 437 $m^2/g$, which is in accordance with the measured areas for the mixed oxides, whose values ranging from 420 to 166 $m^2/g$.

**Table 1**
Summary of characterization results.

| Sample | Particle size (nm)[a] | Phase composition | $S_{BET}$ ($m^2/g$) | Vp ($cm^3/g$)[b] | Dp (nm)[b] | Eg (eV) |
|---|---|---|---|---|---|---|
| TS1-500-clor | 7.6 | Anatase 100% | 420 | 0.255494 | 2.8 | 3.29 |
| TS1-700-clor | 7.9 | Anatase, traces brookite, and rutile | 322 | 0.206587 | 2.9 | 3.16 |
| TS1-500-ace | 10.6 | Anatase 100% | 349 | 0.360055 | 5.7 | 3.53 |
| TS1-700-ace | 11.9 | Anatase 100% | 320 | 0.466730 | 6.3 | 3.39 |
| TS1-500-sul | – | Amorphous | 166 | 0.143852 | 3.6 | 3.16 |
| TS1-700-sul | 21.4 | Anatase 100% | 224 | 0.397943 | 5.8 | 3.31 |

[a] Calculated by the Scherrer equation.
[b] Calculated by BJH method applied to the desorption isotherm.

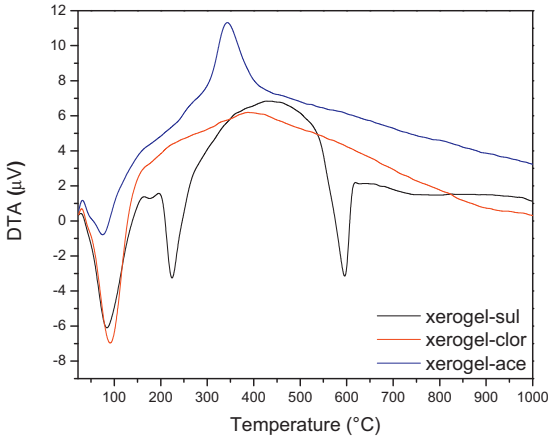


**Fig. 2.** Differential thermal analysis (DTA) curves of the indicated xerogel samples.

In spite of the high calcination temperatures, the mixed oxides exhibit high surface areas, which can be associated again to the dispersive effect of silica. $SiO_2$ acts as a carrier for $TiO_2$, which can help to obtain and keep a large surface area [24]. These results are well correlated with the difference in the anatase crystallite sizes observed for the mixed oxides, as it can be seen in Table 1.

The effect of the temperature on the surface area is more pronounced in the materials obtained with hydrochloric acid. The pore volume decreases from 0.255 to 0.207 $cm^3/g$ with the increasing of the temperature, indicating loss of microporisity. The mean pore diameter remains stable (2.8 nm) since it belongs to the mesopore range. In contrast, both the volume and pore diameter increases with raising temperature in the mixed oxides synthesized with acetic and sulfuric acids, which is consistent with what was found in DRX analysis: increasing temperature allows obtaining a better crystallized structure due to, among others, loss of carbonaceous residues and anions residuals from the synthesis.

The mixed oxides obtained exhibit a type IV isotherm (data not shown), characteristic of mesoporous solids, which is consistent with the behavior of silica. Similarly, the pore sizes of the obtained oxides are at the lower limit of the mesopore range, between 2–6 nm. On the other hand, the hysteresis loop is compatible with type H2 (according with IUPAC classification).

Fig. 2 shows the DTA analyses of the fresh catalysts (xerogels). The mixed oxide obtained with HCl exhibits an endothermic event at *ca.* 90 °C, which can be ascribed to the evaporation of the physisorbed water and to the volatilization of the remaining solvent from the synthesis. The weight loss associated with this event was about 18% (thermogravimetric data not shown for the sake of brevity). It is observed a little exothermic peak around 240 °C that can be assigned to the loss of the hydroxyl groups from incomplete reactions of hydrolysis and condensation. It is also observed an exothermic peak around 400 °C corresponding to the crystallization of the amorphous oxide into anatase crystalline phase.

DTA analysis for the xerogel obtained with acetic acid shows an endothermic peak at 90 °C which is consistent with the volatilization of physisorbed water and the organic solvent (weight loss of 13% between 25–120 °C). It is clearly observed an exothermic peak at *ca.* 360 °C that can be assigned to the combustion of the acetate ligand (weight loss 5%). Phase transition from amorphous to anatase takes place concomitant with the loss of the acetate group, being both events of the same nature (exothermic). Above 500 °C no peaks were observed which could be attributed to the phase transition from anatase to rutile. As a matter of fact, XRD spectra for the oxide TS1-700-ace shows anatase as the only crystalline phase.

DTA for the mixed oxide obtained with sulfuric acid exhibits three main thermal events, each one of them well correlated with significant weight losses in the thermogravimetric analysis. The first one is an endothermic peak assigned to the evaporation of the solvent and the physisorbed water at *ca.* 90 °C (weight loss 18% between 25–150 °C). The second event has an endothermic character and exhibits a maximum peak around 225 °C which might be attributed to the evaporation of the free sulfate groups and not to sulfuric acid because it has a boiling point of 340 °C. The weight loss between 190–260 °C was about 13%. The third endothermic event is observed between 530–620 °C, with a maximum located at *ca.* 595 °C. This event could be ascribed to the loss of sulfate ions strongly anchored to the oxide structure. Yang et al. [25] reported the same behavior for the system $SO_4^{2-}/TiO_2–SiO_2$.

Fig. 3(a) shows IR absorption spectra for the samples synthesized with acetic acid, in the frequency range between 4000–400 $cm^{-1}$. Absorption bands located at 802 and 1079 $cm^{-1}$ are assigned to the symmetric and asymmetric stretching vibrations of Si—O—

Si bonds, respectively, while bands at 462 $cm^{-1}$ could be ascribed to the bending modes of Si—O—Si bonds. In the range between 600–400 $cm^{-1}$ it can also be observed the stretching vibration of Ti—O bonds in Ti—O—Ti groups. Bands at 1631 and 3426 $cm^{-1}$ are attributed to the bending and stretching vibration modes, respectively, of the OH groups of water molecules occluded in the catalyst. The band at 951 $cm^{-1}$ is commonly assigned to the vibration of Si—O—Ti bonds and therefore can be considered as an evidence of the existence of this kind of bonds [26].

Fig. 3(b) shows the infrared spectra of the sulfated catalysts in the frequency range 2000–400 $cm^{-1}$. Infrared spectra of the sulfated metallic oxides usually exhibit absorption bands among 1400–1000 $cm^{-1}$. In the mixed oxide calcined at 500 °C (TS1-500-sul) two absorption bands located at 1230 and 1137 $cm^{-1}$ are clearly observed, which can be ascribed to the presence of $SO_4^{2-}$ ions bonded bidentally. It has been reported that sulfated species like $TiO_2/SO_4^{2-}$ and $SiO_2/SO_4^{2-}$ exhibit absorption bands located around 1375 and 1410 $cm^{-1}$ [27]. Such bands are not observed in the mixed oxide structure because sulfate groups could be covalently linked to the mixed oxide, according with the structure proposed by Yang et al. [25]. This observation is in good agreement with the fact that the characteristic band of Si—O—Ti bonds appears shifted toward lower frequencies (911 $cm^{-1}$) than the band assigned to the catalyst TS1-700-sul (942 $cm^{-1}$), which at the same time exhibits a higher intensity.

Characteristic absorption bands of hydroxyl groups linked to the mixed oxide structure markedly increase their intensity in the catalyst calcined at 700 °C, indicating that sulfate groups not only preserve the anatase crystalline phase, but also prevent the sintering process avoiding in this way the loss of OH groups.

Fig. 3(c) shows the infrared spectra of the mixed oxides obtained with hydrochloric acid. Spectrum of the $SiO_2$ blank is also shown. In a qualitative way, it can be observed that by raising the calcination temperature from 500 to 700 °C the bands located at 3448 and 1633 $cm^{-1}$, from the hydroxyl groups, decrease significantly. The band corresponding to the vibration of Si—O—Ti bonds also decreases its intensity. $TiO_2–SiO_2$ materials obtained with HCl are more affected by the calcination temperature, losing hydroxyl groups, heterolinkages Si—O—Ti and surface area. Infrared spectrum of $SiO_2$ shows the characteristic bands associated with this kind of materials: symmetric and asymmetric stretching vibrations of Si—O—Si bonds (800 and 1079 $cm^{-1}$, respectively) and the bands corresponding to the bending modes of Si—O—Si bonds (460 $cm^{-1}$). It can be observed that these bands markedly decrease their intensity in the mixed oxides due to the interaction of titania and silica. The band assigned to the Si—OH bonds in $SiO_2$ (960 $cm^{-1}$) increases its intensity in the mixed oxides, especially in the sample TS1-500-clor, due to the formation of the Ti—O—Si linkages that absorbs at the same frequency.

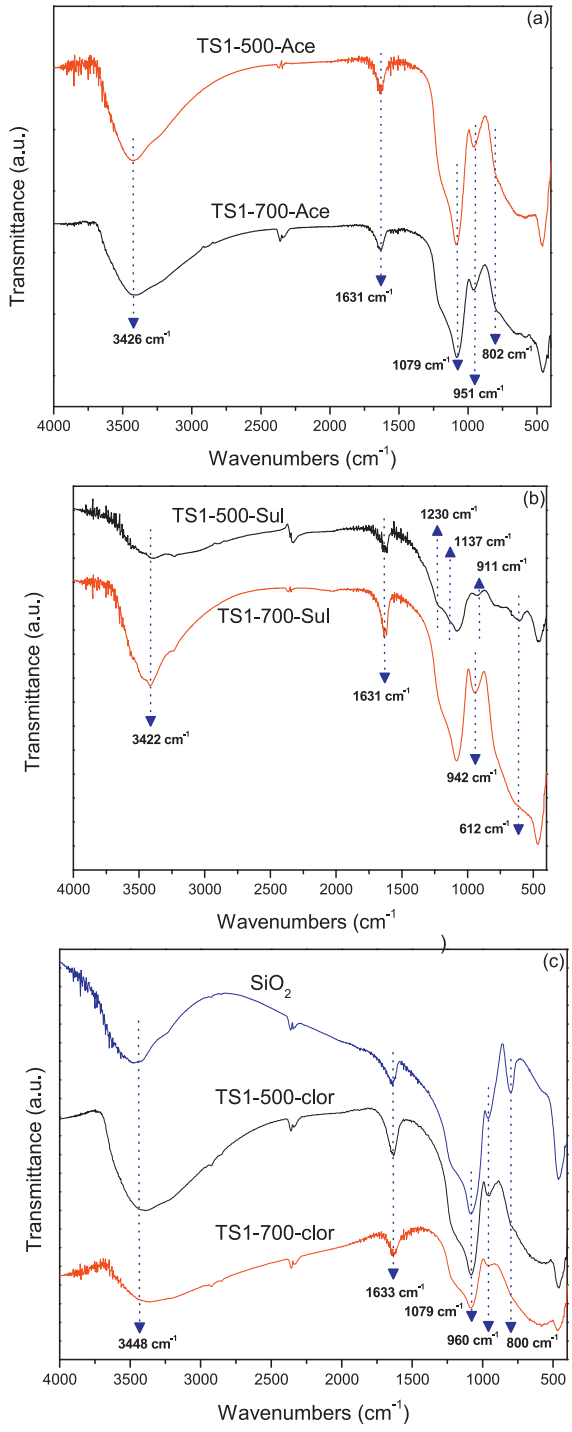


**Fig. 3.** IR spectra of the indicated samples synthesized with: (a) acetic acid, (b) sulfuric acid, (c) hydrochloric acid and $SiO_2$ blank.

Fig. 4 shows the diffuse reflectance UV–vis spectra of the mixed oxides. Values of Eg, the band gap of the catalysts, were derived from the spectra recorded by plotting $(F(R)h\nu)^{1/2}$ vs. $h\nu$, following the method proposed by Tandom and Gupta [19]. The obtained values are reported in Table 1. Pure $SiO_2$ phase does not exhibit absorption in the wavelengths studied (200–500 nm), consequently absorption properties observed are completely due to titania. It must be taken into account that band gap values are conditioned by the existence of crystalline defects and impurities, the preparation method, the average crystal size and, of course, by the method of calculating the values [24].

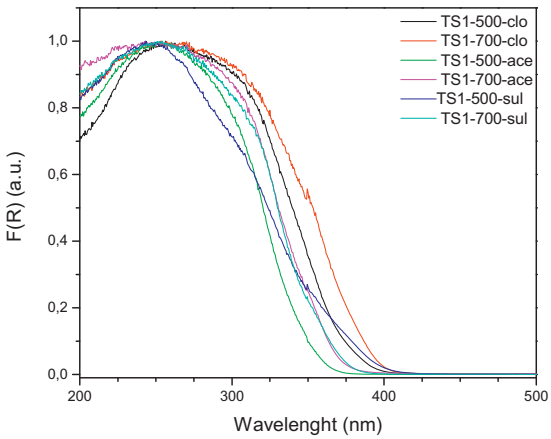


**Fig. 4.** DR-UV/vis spectra of the indicated samples.

Band gap energy values obtained were higher than those for pure $TiO_2$. This can be explained in terms of the effect of silica support and the presence of Ti—O—Si chemical bonds [28] (as we effectively established in the infrared analysis) and they also can be ascribed to the quantum size effect. The calculated band gaps for these materials show a behavior which is dependent on the crystallite size of the $TiO_2$ particles, as it can be observed in Table 1. Band gap increases with decreasing particle size. This behavior is observed either in each pair of mixed oxides (calcined at 500 and 700 °C) obtained with hydrochloric and acetic acid. This behavior, in which the semiconductor band gap increases as the particle size decreases, has been widely discussed and explained by means of a phenomenon called quantum size effect, which is commonly observed in semiconductor particles of a few nanometers. The increase in the band gap occurs as a consequence of the quantization of the particle size, leading to a blue-shift in the absorption spectrum. A similar behavior was observed by Li et al. [29] in titania–silica oxides synthesized by means of sol–gel-hydrothermal and sol–gel synthesis. The quantum size effect is frequently observed in $TiO_2$–$SiO_2$ materials for the effect of the support [30,31].

These observations could not be extended to the samples synthesized with sulfuric acid, since at 500 °C the sample TS1-500-sul is still amorphous. The calculated Eg value for this oxide is lower due to the presence of sulfate groups, which induce a slight shift in the absorption edge towards the visible region, while the sample TS1-700-sul has a higher Eg value, possibly due to the anatase crystalline phase and the silica support.

### 3.2. Photocatalytic activity on the phenol degradation

The photocatalytic behavior of the synthesized samples on the phenol degradation is shown in Fig. 5(a) and (b). Dark oxidation tests as well as photolysis reactions did not show any change in the initial concentration of phenol. Sample TS1-500-clor exhibits the best photocatalytic behavior within the mixed oxides calcined at 500 °C, followed by the mixed oxide TS1-500-ace. Both of them achieved full phenol degradation in 2 h, but the reaction rate was higher with the catalyst TS1-500-clor. TS1-500-sul did not show a good performance, a fact that can be explained in terms of its high degree of amorphicity, according with the XRD spectra. At 700 °C, all oxides show a notable improvement in the activity except the sample prepared with hydrochloric acid in which the conversion strongly decays probably due to the significant reduction of surface area (Table 1). The best photocatalytic performance was achieved with the mixed oxide TS1-700-ace, as it can be seen in Fig. 5(b).

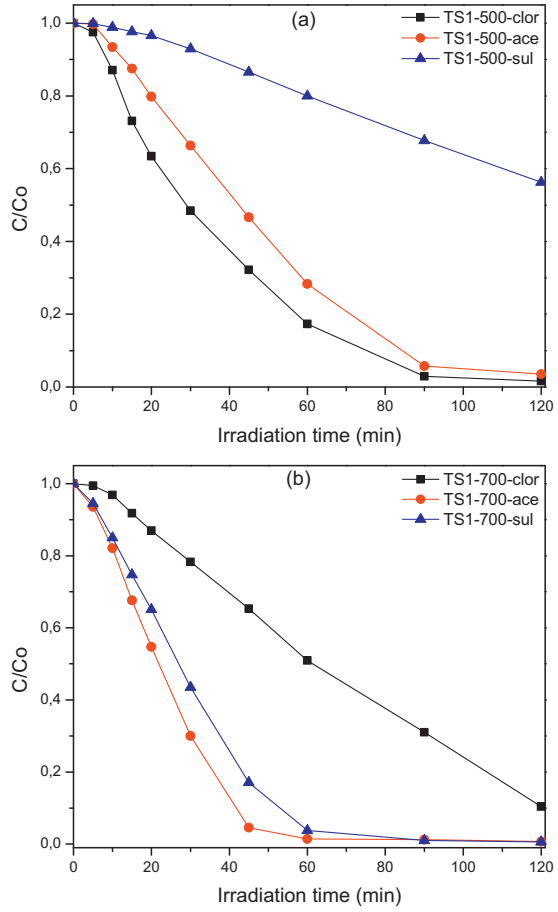


**Fig. 5.** Photocatalytic performance of the titania–silica mixed oxides calcined at: (a) 500 °C, (b) 700 °C.

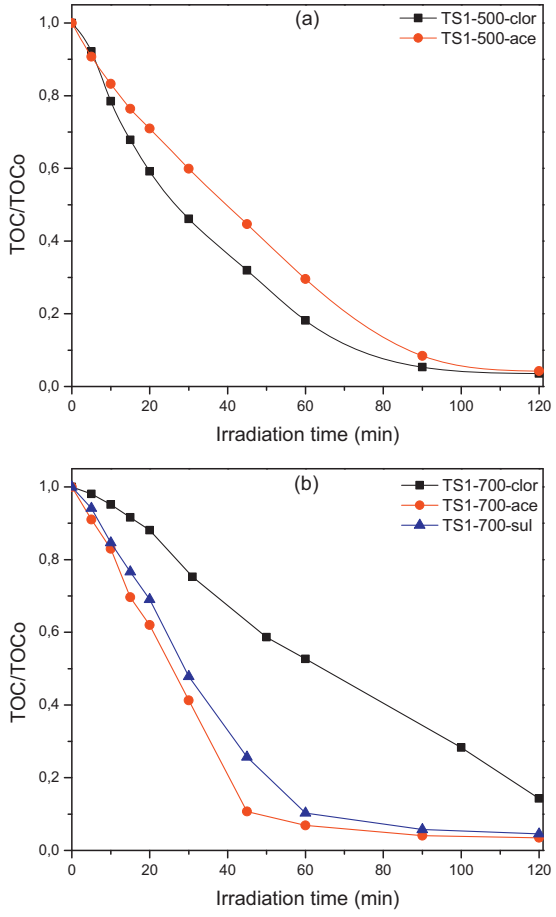


**Fig. 6.** Evolution of the total carbon content in the reaction mixture by the mixed oxides calcined at: (a) 500 °C, (b) 700 °C.

It has been widely recognized that the photocatalytic activity of $TiO_2$ depends on factors such as crystal structure, surface area, crystallite size, and surface hydroxyl groups. The crystalline phase is one of the most important parameters, and it is generally accepted that anatase phase is the most photoactive polymorph of $TiO_2$ ascribed to its higher adsorption affinity to organic compounds, its high surface area and, unlike rutile, it exhibits a reduced rate of electron–hole recombination [32]. These properties can be modified by the method of synthesis, the precursors used, the type of acid and the eventual addition of modifying agents.

The mixed oxides obtained with hydrochloric acid were composed of anatase crystalline phase with traces of brookite and rutile. The presence of the other two polymorphs of $TiO_2$ is ascribed to the $Cl^-$ anion in a highly acidic environment. The stabilizing role of the silica was reflected not only by limiting the effect of the anion avoiding the formation of a higher proportion of brookite and rutile, but also by retarding the sintering process, preserving the anatase phase and limiting the loss of surface area. Photocatalytic activity of the mixed oxide calcined at 700 °C decreased with respect to that calcined at 500 °C, which can be attributed mainly to the loss of surface area. As we discuss above, surface area as well as pore volume decreased significantly in the mixed oxide TS1-700-clor, resulting in a material with a lower capacity of adsorption. Besides, the pore diameter of this material was the smallest of all oxides calcined at 700 °C. Infrared spectra also showed a reduction in the Si—O—Ti heterolinkages, which are widely accepted as responsible of the great catalytic properties exhibited by the mixed oxides in a wide range of reactions [33].

On the other hand, acetic acid has been used as a stabilizing agent in the sol–gel synthesis since this compound reacts at atomic level with the titanium alkoxide to give a new precursor, according with Eq. (1) [14]:

$$Ti(OPr^i) + CH_3COOH \rightarrow Ti(OPr^i)_3OOCCH_3 + Pr^iOH \quad (1)$$

The Ti coordination number increases from 4 to 5. In this sense, the reaction of titanium alkoxide with the acetate ligand coupled to its steric effect give a decrease of the rate of hydrolysis of the Ti alkoxide. Acetate ligands are stable until temperatures close to 400 °C, for this reason the anatase crystalline phase can be preserved since the crystallization process begins when acetate groups are completely loss. A further increase in the photocatalytic activity with the calcination temperature can be explained taking into account the stability provided by the acetate ligand and the silica support, because of this the crystallization process takes place in a wide range of temperatures. Even though the XRD pattern of the catalyst TS1-500-ace showed anatase as the only crystalline phase, a further increase in the temperature allowed obtaining a better crystallized anatase phase. In addition, increasing the calcination temperature permitted removing carbonaceous residues from the acetate anion and impurities from the sol–gel process, which could be blocking active sites. This could explain the fact that the initial reaction rate of the catalyst TS1-700-ace was doubled compared with that observed in catalyst TS1-500-ace. Another evidence of the change in the crystalline structure of $TiO_2$ with increasing the calcination temperature is the Eg value. Eg values for samples synthesized with acetic acid decreased from 3.53 to 3.39

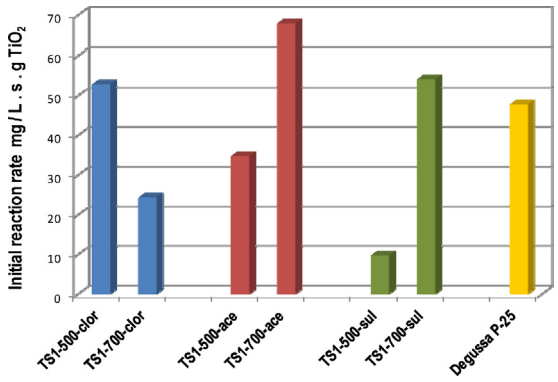


**Fig. 7.** Initial reaction rate per gram of active phase for phenol photooxidation for the indicated catalysts. $[Phenol]_0 = 50$ mg/L, $V = 0.45$ L, [Catalyst] = 1 g/L, Photon flux $\sim 2.6 \times 10^{-7}$ Einstein $s^{-1}$ $L^{-1}$.

as the calcination temperature increased, which could be ascribed, in part, to a better crystallized anatase structure.

The sulfated mixed oxide calcined at 700 °C (TS1-700-sul) shows a substantial increase in the phenol degradation with respect to that calcined at 500 °C (TS1-500-sul). This latter material is almost amorphous and has a lower surface area, which can explain its lower activity. On the contrary, sample TS1-700-sul exhibits a well crystallized anatase phase and a higher surface area, which is consistent with its better photocatalytic performance. Nevertheless, the photocatalytic properties of the sample TS1-700-ace remain higher.

Fig. 6 shows the evolution of the TOC (total organic carbon) for the samples calcined at 500 °C (data not shown for sample TS1-500-sul) and 700 °C. It can be seen that these TOC profiles match the profiles for the phenol degradation (Fig. 6(a) and (b)). This means that phenol is being mineralized (converted to $CO_2$) almost completely. For instance, at 2 h the phenol degradation with the catalyst TS1-700-clor was 90%, while the mineralization of organic matter was about 85%.

Fig. 7 shows a comparison of the initial reaction rates of phenol degradation per gram of photocatalytic oxide ($TiO_2$). It can be observed that each type of acid used leads to photocatalysts with higher activity than Degussa P-25. Under this scenario the photocatalytic activity of the catalyst TS1-700-ace is clearly superior. It has to be also taken into account that the decantability properties of the mixed oxides are much better than those of Degussa P25, thus facilitating the recovering of the former after the photocatalytic reactions.

## 4. Conclusions

$TiO_2$–$SiO_2$ mixed oxides with high photocatalytic activity were synthesized by the sol–gel technique. The effect of three different acids was analyzed and the results showed that the kind of acid used during the preparation strongly influences the phase composition and stability of the $TiO_2$ phases incorporated in the silica structure as well as the photocatalytic activity. Thus, $SO_4^{2-}$ and $CH_3COO^-$ ions stabilized the anatase phase at high calcination temperatures (700 °C) leading to samples with the highest photoactivities.

The highest photoactivity in the reaction of phenol photooxidation was achieved with the catalyst TS1-700-ace, due to a combination of factors like high surface area, large crystallite size and the presence of anatase crystalline phase, in which the role of the silica as a stabilizing agent was a crucial issue to preserve these properties at high calcination temperatures. It was also remarkable the function of the acetate ligand stabilizing the crystalline anatase phase. The photocatalytic performance of this material was quite superior to that obtained with the commercial catalyst Degussa P-25.

## Acknowledgements

Thanks are given to “Instituto de Ciencia de los Materiales de Sevilla, CSIC-Universidad de Sevilla”, to “Ministerio de Ciencia e Innovación de España”, to “Universidad de Antioquia, Comité para el Desarrollo de la Investigación–CODI” and to “Departamento Administrativo de Ciencia, Tecnología e Innovación (Colciencias)–Programa de Doctorados Nacionales 2004” for financial support. Thanks are also given to Gloria Restrepo and Juan Miguel Marín who accepted the author Biviana Llano for the PhD position that lead to these results.

## References

[1] B. Tian, F. Chen, J. Zhang, M. Anpo, J. Colloid Interface Sci. 303 (2006) 142–148.
[2] K. Yanagisawa, J. Ovenstone, J. Phys. Chem. B 103 (1999) 7781–7787.
[3] Z. Wang, D. Xia, G. Chen, T. Yang, Y. Chen, Mater. Chem. Phys. 111 (2008) 313–316.
[4] A. Pottier, C. Chanéac, E. Tronc, L. Mazerolles, J.P. Jolivet, J. Mater. Chem. 11 (2001) 1116–1121.
[5] J.H. Lee, Y.S. Yang, J. Eur. Ceram. Soc. 25 (2005) 3573–3578.
[6] A. Di Paola, G. Cufalo, M. Addamo, M. Bellardita, R. Campostrini, M. Ischia, R. Ceccato, L. Palmisano, Colloids Surf. A: Physicochem. Eng. Aspects 317 (2008) 366–376.
[7] G. Colón, M.C. Hidalgo, J.A. Navío, Appl. Catal. B: Environ. 45 (2003) 39–50.
[8] G. Colón, M.C. Hidalgo, G. Munuera, I. Ferino, M.G. Cutrufello, J.A. Navío, Appl. Catal. B: Environ. 63 (2006) 45–59.
[9] D.S. Muggli, L. Ding, Appl. Catal. B: Environ. 32 (2001) 181–194.
[10] G. Colón, M.C. Hidalgo, J.A. Navío, A. Kubacka, M. Fernández-García, Appl. Catal. B: Environ. 90 (2009) 633–641.
[11] H. Li, G. Li, J. Zhu, Y. Wan, J. Mol. Catal. A: Chem. 226 (2005) 93–100.
[12] J.A. Chang, M. Vital, I.C. Baek, S.I. Seok, J. Solid State Chem. 182 (2009) 749–756.
[13] C. Guillard, B. Beaugiraud, C. Dutriez, J.M. Herrmann, H. Jaffrezic, N. Jaffrezic-Renault, M. Lacroix, Appl. Catal. B: Environ. 39 (2002) 331–342.
[14] A.S. Attar, M.S. Ghamsari, F. Hajiesmaeilbaigi, S. Mirdamadi, J. Mater. Sci. 43 (2008) 1723–1729.
[15] X. Gao, I.E. Wachs, Catal. Today 51 (1999) 233–254.
[16] Z.Y. Wu, Y.F. Tao, Z. Lin, L. Liu, X.X. Fan, Y. Wang, J. Phys. Chem. C 113 (2009) 20335–20348.
[17] J. Aguado, R. van Grieken, M.J. López-Muñoz, J. Marugán, Appl. Catal. A: Gen. 312 (2006) 202–212.
[18] E. Beyers, E. Biermans, S. Ribbens, K. De Witte, M. Mertens, V. Meynen, S. Bals, G. Van Tendeloo, E.F. Vansant, P. Cool, Appl. Catal. B 88 (2009) 515–524.
[19] S.P. Tandom, J.P. Gupta, Phys. Stat. Sol. 38 (1970) 363–367.
[20] M. Zhang, L. Shi, S. Yuan, Y. Zhao, J. Fang, J. Colloid Interface Sci. 330 (2009) 113–118.
[21] V. Brezová, A. Blazková, L. Karpinský, J. Grosková, B. Havlínová, V. Jorík, M. Ceppan, J. Photochem. Photobiol. A: Chem. 109 (1997) 177–183.
[22] C.H. Chiou, C.Y. Wu, R.S. Juang, Chem. Eng. J. 139 (2008) 322–329.
[23] Z. Whang, D. Xia, G. Chen, T. Yang, Y. Chen, Mater. Chem. Phys. 111 (2008) 313–316.
[24] B. Llano, G. Restrepo, J.M. Marín, J.A. Navío, M.C. Hidalgo, Appl. Catal. A: Gen. 387 (2010) 135–140.
[25] H. Yang, R. Lu, L. Wang, Mater. Lett. 57 (2003) 1190–1196.
[26] Z.Y. Liu, X. Quan, H.B. Fu, X.Y. Li, K. Yang, Appl. Catal. B 52 (2004) 33–40.
[27] S.M. Jung, O. Dupont, P. Grange, Appl. Catal. A: Gen. 208 (2001) 393–401.
[28] T. Ohno, S. Tagawa, H. Itoh, H. Suzuki, T. Matsuda, Mater. Chem. Phys. 113 (2009) 119–123.
[29] Z. Li, B. Hou, Y. Xu, D. Wu, Y. Sun, W. Hu, F. Deng, J. Solid State Chem. 178 (2005) 1395–1405.
[30] J. Marugán, M.J. López-Muñoz, R. van Grieken, J. Aguado, Ind. Eng. Chem. Res. 46 (2007) 7605–7610.
[31] G. Lassaletta, A. Fernandez, J.P. Espinos, A.R. Gonzalez-Elipe, J. Phys. Chem. 99 (1995) 1484–1490.
[32] S. Sakthivel, M.C. Hidalgo, D.W. Bahnemann, S.-U. Geissen, V. Murugesan, A. Vogelpohl, Appl. Catal. B: Environ. 63 (2006) 31–40.
[33] H.S. Kibombo, R. Peng, S. Rasalingam, R.T. Koodali, Catal. Sci. Technol. 2 (2012) 1737–1766.